Flow Effects on the Controlled Growth of Nanostructured Networks at Microcapillary Walls for Applications in Continuous Flow Reactions

Gang Wang,[†] Cansheng Yuan,[§] Boyi Fu,[§] Luye He,[§] Elsa Reichmanis,*,[§,||,⊥] Hongzhi Wang,*,[†] Qinghong Zhang,[‡] and Yaogang Li*,[‡]

[†]State Key Laboratory for Modification of Chemical Fibers and Polymer Materials, College of Material Science and Engineering, and [‡]Engineering Research Center of Advanced Glasses Manufacturing Technology, MOE, Donghua University, Shanghai 201620, People's Republic of China

[§]School of Chemical and Biomolecular Engineering, [||]School of Chemistry and Biochemistry, and [⊥]School of Materials Science and Engineering, Georgia Institute of Technology, Atlanta, Georgia 30332, United States

S Supporting Information

ABSTRACT: Low-cost microfluidic devices are desirable for many chemical processes; however, access to robust, inert, and appropriately structured materials for the inner channel wall is severely limited. Here, the shear force within confined microchannels was tuned through control of reactant solution fluid-flow and shown to dramatically impact nano- through microstructure growth. Combined use of experimental results and simulations allowed controlled growth of 3D networked Zn(OH)F nanostructures with uniform pore distributions and large fluid contact areas on inner microchannel walls. These attributes facilitated subsequent preparation of uniformly distributed Pd and PdPt networks with high structural and chemical stability using a facile, in situ conversion method. The advantageous properties of the microchannel based catalytic system were demonstrated using microwave-assisted continuous-flow coupling as a representative reaction. High conversion rates and good recyclability were obtained. Controlling materials nanostructure via fluid-flow-enhanced growth affords a general strategy to optimize the structure of an inner microchannel wall for desired attributes. The approach provides a promising pathway toward versatile, high-performance, and low-cost microfluidic devices for continuous-flow chemical processes.

KEYWORDS: shear stress, 3D networks, flow chemistry, microfluidic reactions
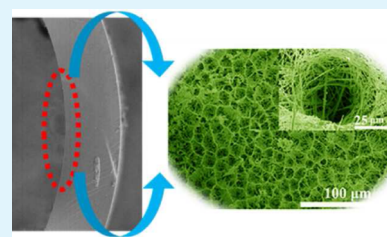
1. INTRODUCTION

Continuous-flow chemical processing using microfluidic devices has significant potential in organic synthesis and nano-technology for applications ranging from pharmaceuticals to electronics and photonics.[1−4] The confined channel offers many advantages, including minimal or no micro/nanostructure damage during functionalization and integration, and risks associated with leakage of reagents can be eliminated.[5−9] Other important benefits comprise safety, reproducibility, rapid heat and mass transfer, and ease of automation.[10] Moreover, purification steps could be avoided and the flow reactors could be used repeatedly, thereby reducing overall production cost.[11−13]

Full utilization of the capabilities promised by such systems requires optimization of the material, and its requisite nanostructure, that embodies the inner channel wall.[14,15] Because it is in direct contact with the reaction fluid, the material must itself be inert. Then, for many chemical processes, a surface structure that facilitates large fluid contact area is desirable.[16−18] Further, the microstructure must be uniform throughout the length of the channel. One example in which a microchannel that exhibits large fluid contact area and uniform distributions would be highly desirable is in catalytic

processes. Noble metals and alloys are among the most widely used materials for organic catalysis but high economic cost restricts their use.[19−21] To ameliorate cost, catalysts are often incorporated onto alternative supports.[22−25] To be effective in a continuous-flow microchannel, the catalyst should possess a large effective fluid contact area, be distributed uniformly and be stable under fluid errosion.[26−29] These requirements are exceptionally difficult to achieve using the traditional approach that simply incorporates the noble metal onto a packing medium.[30,31] Thus, there is significant interest in the design and development of alternative three-dimensional (3D) structures to support noble metal networks.

Recently, several complex lithographic approaches to the fabrication of 3D nanostructured microfluidic channels have been reported for a range of applications, including catalyst support structures.[32,33] However, direct and facile access to suitable 3D networked structures within confined micro-channels continues to be challenging. An approach that has not been extensively investigated involves the use of fluid flow.

Under microfluidic conditions, laminar shear stress will occur along with laminar fluid flow. While shear stress or fluid flow have been widely used in materials processing for applications aiming to effect polymer chain alignment, inorganic fiber and film orientation, and crystallization of molecules;[34−37] reports related to the effects of fluid flow on microstructure development within confined microchannels are limited, especially as they relate to the controllable growth of nanostructured networks.[38,39]

Here, fluid shear-induced microstructured growth of Zn-(OH)F within a confined microchannel was achieved for the first time. Zn(OH)F was selected because (i) it is known to be inert, (ii) it can be readily grown on glass and polymer substrates, and (iii) deposition onto the inner wall of microcapillaries is feasible. A wide range of structures were accessible, under controllable and importantly, reproducible conditions. Upon optimization, robust 3D networked nanostructures with uniform pore distributions and large fluid contact areas were readily achieved. Subsequently, in situ conversion of commensurate precursor solutions produced uniformly distributed catalytic Pd and PdPt networks in a facile manner. The efficacy of the network catalysts was demonstrated for coupling reactions in a continuous-flow, microwave assisted system. Reaction rates were significantly enhanced, and the microchannel catalytic substrates were recyclable.

These results improve significantly upon current microfluidic technology, and show promise for applications in continuous flow reactions. Microchannels modified with 3D noble metal networks may also find application in areas such as microreactors, photocatalysis, and energy harvesting because of their large contact surface area, excellent structural stability, resistance to erosion under fluid flow, and acceleration of reaction efficiency.

2. EXPERIMENTAL SECTION

2.1. Reagents and Materials. All chemicals and reagents were purchased in the highest commercially available grade and were used without further purification. Zinc nitrate, ammonium fluoride, hexamethylenetetramine, and sodium citrate dihydrate were purchased from Sinopharm Chemical Reagent Co., Ltd. Potassium chloropalladite (K_2PdCl_4) and potassium tetrachloroplatinate (II) (K_2PtCl_4) were purchased from Alfa Aesar Co., Ltd. Glass capillaries (Jianuo Chromatography Inc., Nanjing, China) with were used as microchannels.

2.2. Characterization. Transmission electron microscopy (TEM) and high-resolution TEM (HRTEM) images were obtained using a JEM-2100F transmission electron microscope (JEOL, Ltd., Japan) operating at 200 kV. Field emission-scanning electron microscopy (FE-SEM) images were taken on an JSM-6700F FE-SEM (Hitachi, Ltd., Japan) to characterize networks morphologies. FE-SEM samples were prepared by cutting subject capillaries into pieces. Energy dispersive spectrometer (EDS) mapping of each element was obtained using a JSM-6700F field emission-scanning electron microscope equipped with an Oxford Instruments EDS detector. X-ray photoelectron spectra (XPS) were recorded on an ESCALab MKII X-ray photoelectron spectrometer. The fluid simulation results were obtained from the commercial COMSAL 4.4 software.

2.3. Fluid Shear-Induced Microstructure Formation in Confined Microchannels. First, ZnO nanoseeds were fabricated on the inner walls of the microchannels according to literature methods.[6] Next, 3D networks with large surface areas were prepared at 90 °C by pumping the aqueous solution A (a mixture of 0.05 M zinc nitrate and 0.05 M ammonium fluoride with the same volume ratio), and the aqueous solution B (0.05 M hexamethylenetetramine), into the capillary microchannel for about 1.5 h at various pump rates, namely, 10, 30, 50, 70, and 90 μL min⁻¹. After the reaction was

complete, the capillary microchannel was cleaned with distilled water at a flow rate of 25 μL min⁻¹ for 10 min (room temperature, ca. 23 °C), and then dried at 120 °C for 1 h.

2.4. Preparation of Pd and PdPt Mono/Multimetallic Networks. In a typical synthesis of Pd and PdPt mono/multimetallic networks, 4 mL of an aqueous solution of monometal (6 mM K_2PdCl_4) or multimetal precursor (a mixture of 6 mM K_2PdCl_4 and 6 mM K_2PtCl_4 with the same volume ratio) was added to an aqueous solution of sodium citrate dihydrate (0.06 mL, 60 mM). Subsequently, the resulting solution was injected into the 3D network modified microchannels at ca. 90 °C in a continuous manner at a flow rate of 10 μL min⁻¹ for about 20 min. The apparatus was maintained in a convection oven during the course of the reaction. After the reaction was completed, the microchannels were washed with ethanol at a flow rate of 10 μL min⁻¹ for 10 min at 25 °C and then dried in a convection oven at 100 °C for about 30 min.

2.5. Continuous-Flow Microwave Assisted Cross-Coupling Reaction. Reaction solutions containing aryl iodide (1.0 mmol, 1.0 equiv), acrylate (1.3 mmol, 1.3 equiv), and triethylamine (3.0 mmol, 3.0 equiv) in 1.5 mL of dimethylformamide (DMF) were flowed through a single inlet into the modified capillary while being irradiated. The continuous-flow microwave reaction system was assembled as shown in Figure S9. The capillary microchannel with the immobilized 3D Pd network was attached to a Y-shaped connector, which was connected to two polytetrafluoroethylene tubes. Solutions of the reaction reagents in organic solvents (details can be found in the Supporting Information) were introduced using syringes under the control of two syringe pumps. All catalysis experiments were conducted at a microwave frequency of 2.45 GHz with a power between 0 and 300 W. The microwave assisted flow-chemistry experiments were carried out in a CEM-DiscoverLabMate monomode microwave apparatus equipped with an IntelliVent pressure control system and a vertically focused IR temperature sensor. The outlet from the reactor was collected into a microtube and analyzed by GC-MS spectroscopy (QP-2010, Shimadzu, Japan) immediately after the reaction.

2.6. The Preparation of Pd Catalyst for Batch Reaction. First, 4 mL of an aqueous solution of K_2PdCl_4 (6 mM) was added to an aqueous solution of sodium citrate dihydrate (0.06 mL, 60 mM) to prepare the Pd precursor solution. Subsequently, 0.2 mL of as-prepared Pd precursor solution was injected into the three-neck, round-bottom flask containing 0.2 g of Zn(OH)F at ≈90 °C, and equipped with a Teflon coated magnetic stir bar. The reaction mixture was stirred at ca. 90 °C for about 20 min to ensure all the Pd precursor had reacted. After the reaction was complete, the product was washed at ambient temperature with water (5 mL) three times and dried in a vacuum oven held at ca. 120 °C for 12h.

2.7. Cross-Coupling Reaction in Batch Reactor. Reaction solutions containing aryl iodide (1.0 mmol, 1.0 equiv), acrylate (1.3 mmol, 1.3 equiv), and triethylamine (3.0 mmol, 3.0 equiv) in 1.5 mL of DMF were premixed at ambient temperature. For batch reactions with microwave assistance, the catalyst synthesized as per the above procedure (0.22 g, containing 0.49 mg Pd), the reaction solutions and reaction temperatures were controlled under the same conditions as the corresponding reactions conducted in microfluidic reactors. The catalysts and reaction solutions were then added to a 10 mL Pyrex microwave vial containing a Teflon-coated stir bar and a septum under an argon atmosphere and they were then stirred for 20 s. All microwave irradiation experiments were carried out in a CEM-DiscoverLabMate monomode microwave apparatus equipped with an IntelliVent pressure control system and a vertically focused IR temperature sensor. After the irradiation period, the reaction vessel was cooled rapidly (60−120 s) to ambient temperature by air jet cooling.

3. RESULTS AND DISCUSSION

3.1. Fluid-Flow-Enhanced Zn(OH)F Microstructure Growth. A Zn(OH)F network was fabricated within a microcapillary channel under a range of flow conditions.

Reaction parameters such as temperature and ratio of reagents which are known to be important determinants of resultant structure were kept constant.[7] Field-emission scanning electron microscopy (FE-SEM) (Figure 1) demonstrated the impact reactant solution flow rate has on ensuing Zn(OH)F morphology.
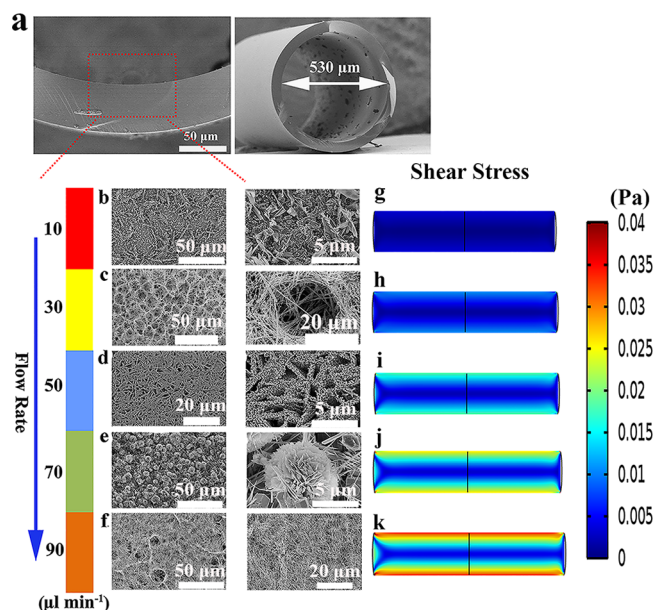

Figure 1. (a) FE-SEM images of the microchannel at different magnifications; (b−f) FE-SEM images of microstructures constructed within confined microchannels at the following fluid flow rates: (b) 10, (c) 30, (d) 50, (e) 70, and (f) 90 μL min^{-1}. (To better observe various morphology size distributions, different scale bars were utilized.) The images on the right (g−k) are the corresponding fluid simulations of the shear stress distributions (shear stresses increase from blue to red in the scale bar).

The fabrication process was carried out in water, the solution is known not to undergo shear-thinning, and thus the fluid was assumed to be Newtonian.[40] Given the 530 μm diameter of the glass capillary, the solution flow rates investigated here varied substantially: 10−90 μL min^{-1} or, alternatively, 4.55−41 cm min^{-1}, respectively. Even at the highest fluid flow rate, the low Reynolds number (Re, ca. 0.05) suggests laminar flow conditions (Re < 2000) over the entire range of rates investigated here. The calculation of Re can be found in the

Supporting Information. To assist evaluation of the impact of the fluid flow environment on resultant Zn(OH)F morphology, a COMSOL laminar flow model was developed to simulate fully developed steady state fluid flow within the microcapillary. The simulation results suggest the evolution of an increased shear force field with increased flow rate, as illustrated in Figure 1g−k. The shear stress is given by eq 1:

$$\tau(r) = \mu \frac{\partial u}{\partial r} \tag{1}$$

where μ is the dynamic viscosity of the fluid, u is the velocity of the fluid along the length of the capillary, and r is the radius from the centerline of the capillary.

Figure 1b−f presents the microstructures obtained with reagent flow rates of 10, 30, 50, 70, and 90 μL min^{-1}, respectively. At a fluid flow rate of only 10 μL min^{-1} (Figure 1b), random microstructures with very limited uniformity were observed. At 30 μL min^{-1}, highly uniform 3D networked structures were obtained. With a further increase (50 μL min^{-1}), a denser, more packed networked structure developed. At 70 and 90 μL min^{-1}, the structures appeared to be highly uniform, flower-like or layered nanowire/nanofiber microstructures orientated along the flow direction. Almost no structure formation was observed with further increases in flow rate, a result attributed to increased shear force (image not shown).

The reaction taking place during microstructure formation is represented by eq 2.

$$Zn^{2+} + F^- + OH^- \leftrightarrow Zn(OH)F \tag{2}$$
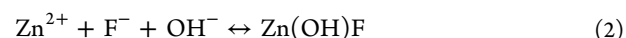
Typically, reaction kinetics is affected by the nature of the reactants, physical state, concentration, temperature, pressure, and the presence of catalysts. All the reaction factors, including the microcapillary inner wall diameter, reaction time, reaction temperature, and reactant composition, were controlled to the same conditions. During the growth process, the fluid velocity, and thus shear stress, was the only variable that was changed. The simulation results (Figure 1g−k), suggest that shear stress and fluid flow rate increase proportionally to first order eq 1. Shear stress had been reported to impact polymer crystallization, nanofiber formation and nanowire orientation;[34−37] the results presented here demonstrate that shear stress associated with fluid flow also plays an important role in microstructure growth and the evolution of materials morphology. Thus, "fluid shear-induced microstructure for-
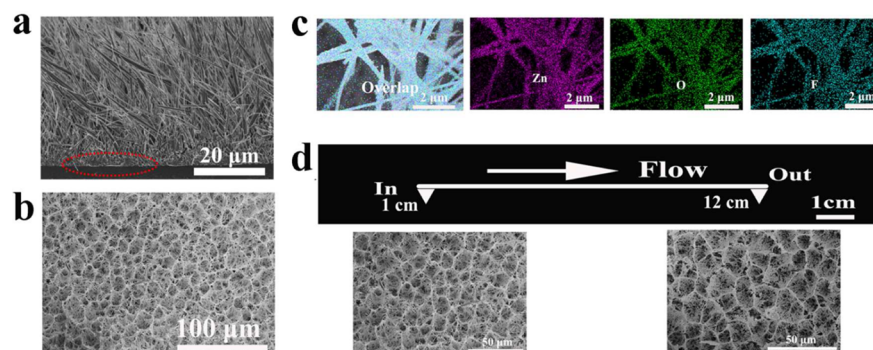

Figure 2. (a−c) Side-view FE-SEM image (the red oval marked the interface between the constructed networks and microchannel inner wall.), top-view FE-SEM image, and elemental mapping images of the constructed 3D networks, respectively; (d) FE-SEM images of the microstructures in different positions of the microchannel.
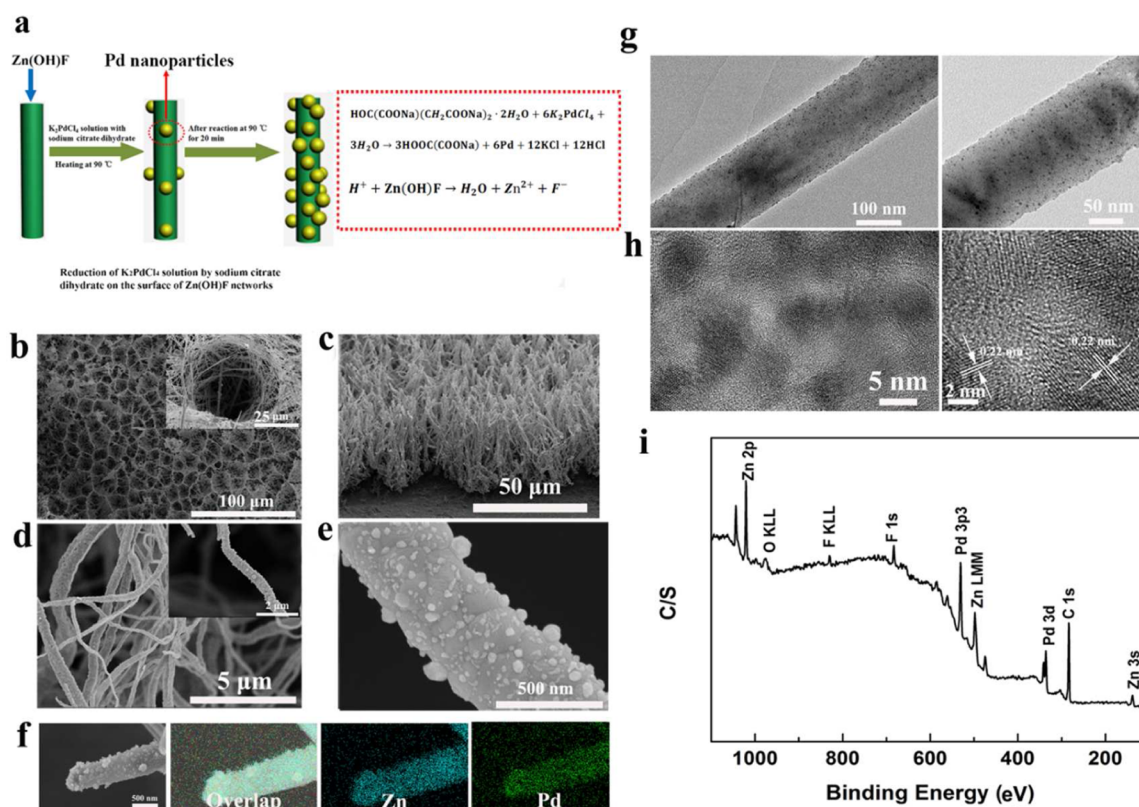
Figure 3. (a) Schematic representation of the 3D Pd network synthesis process. (b) Top-view FE-SEM image (the inset is a magnified image of a pore in the network). (c) Tilted FE-SEM image. (d) Top-view FE-SEM image of the micropores distributed in the network (the inset is a magnified image of a Pd nanowire). (e) High-magnification FE-SEM image of the Pd nanowire. (f) SEM-EDS elemental mapping images of the Pd nanowire. (g) TEM images. (h) HRTEM images. (i) XPS spectrum of the 3D Pd network in a confined microchannel.

mation" may provide a general strategy for the controlled fabrication of a range of structures within confined microchannels.

3.2. Microstructure Analysis of 3D Networks. Close inspection of the structure obtained from a flow rate of 30 μL min^{-1} reveals formation of a continuous, well integrated, approximately 50 μm thick, networklike structure on the inner channel wall (Figure 2a). The red oval identifies the interface between the networked structure and inner wall; as grown Zn(OH)F appears well connected with the channel wall. Further, the network appears to consist of a large number of nanowires with high length-to-diameter ratios. Figure 2b shows that the nanowires comprising the network assemble into larger-scale, somewhat uniform, microporous structures which have a diameter of about 20 μm. High-resolution transmission electron microscopy (HRTEM) provided additional insight into characteristics of the microstructure (see Figure S1 in the Supporting Information).

The nanowires exhibited smooth surfaces with a lattice spacing of 0.22 nm (Figure S1), which corresponds to that of a Zn(OH)F nanocrystal. The elemental distribution within the networked nanowires was determined by elemental mapping analysis using FE-SEM-energy dispersive spectrometry (FE-SEM-EDS) (Figure 2c). Uniform elemental distributions of Zn, O, and F were observed with full overlap of the three elements throughout the nanowire structure, confirming successful growth of Zn(OH)F. As demonstrated through examination of SEM images taken near the inlet and outlet of the capillary (Figure 2d), network growth was reasonably uniform throughout the 12 cm microchannel length.

3.3. In Situ Conversion to Pd Networks. The advantages derived from the present networked Zn(OH)F structure for microfluidic processes was explored using a noble metal catalytic system. Pd decorated networks were produced in situ, via injection of the reaction solution (containing metal precursors and sodium citrate) into the 3D Zn(OH)F network modified microchannel. The apparatus was maintained in a conventional drying oven at a temperature 90 °C, and the solution was injected continuously at a rate of 10 μL min^{-1} for about 20 min. K$_2$PdCl$_4$ and sodium citrate dehydrate were the metal source and reducing agent, respectively.

During flow, Pd nanocrystals formed on the surface of the networked substrate. The proposed reaction scheme is presented in Figure 3a. Additionally, temporal changes in the morphology of the Pd coated nanowires were investigated (Figure S2 in the Supporting Information). The in situ decoration of the Zn(OH)F networked substrate with Pd is attributed to surface etching of the pristine substrate as a result of the increased acidity during the reaction. As the reduction reaction of the metal precursor with citrate proceeds, the pH of the reaction mixture decreases owing to the consumption of OH$^-$ ions through deprotonation of citrate, which is coordinated to the metal precursor (the chemical reactions are shown in Figure 3a).[24]

The Pd nanocrystal modified networks were further characterized by FE-SEM, TEM and X-ray photoelectron spectroscopy (XPS) analysis. Low resolution, top-view FE-SEM imaging (Figure 3b) demonstrates that decoration with Pd did not alter the original network structure, and fluids are expected to flow through the structure with low resistance and large
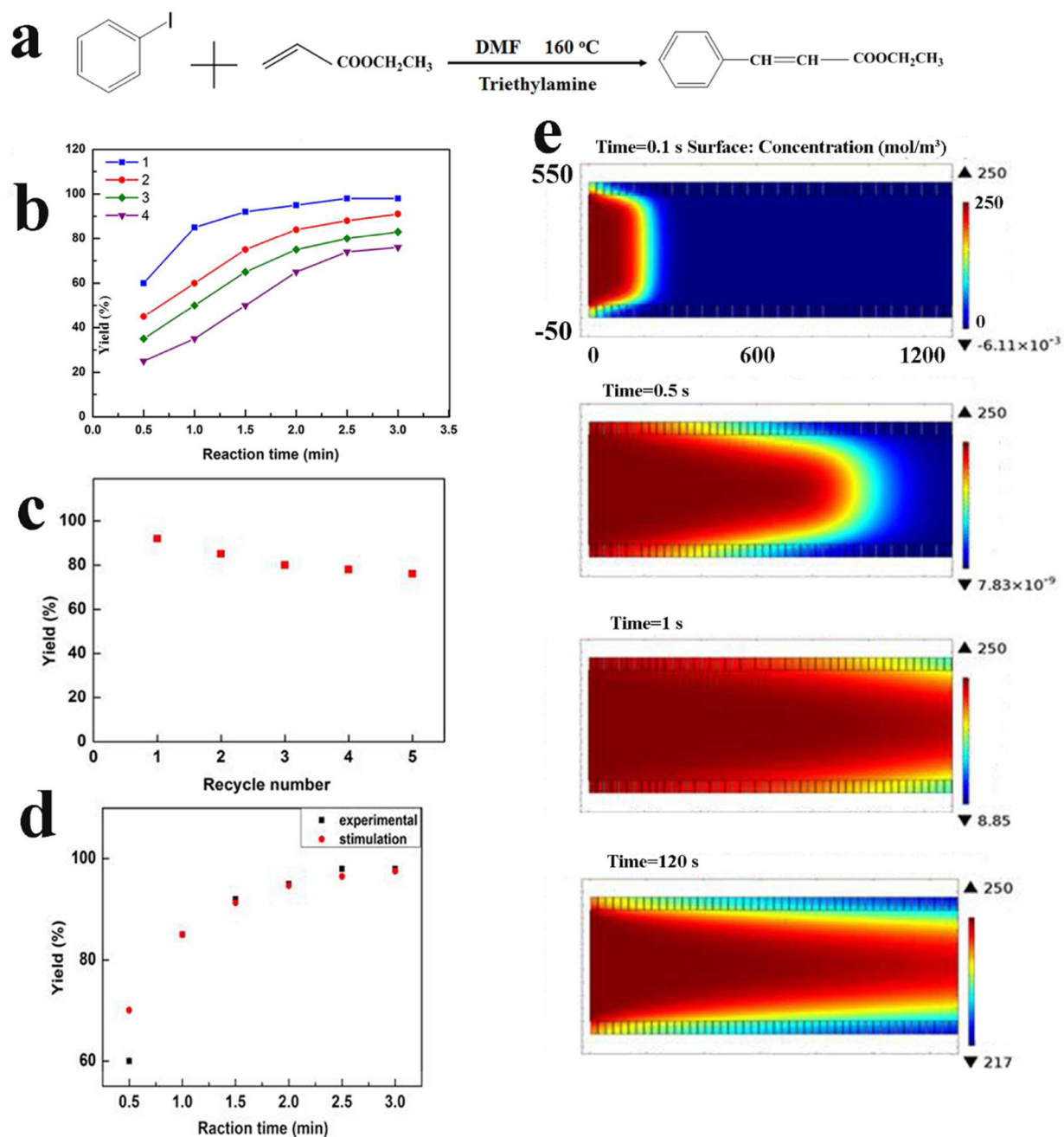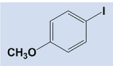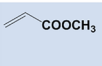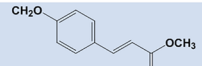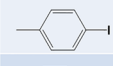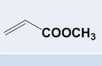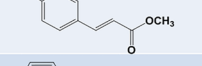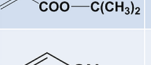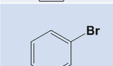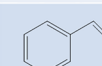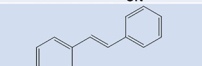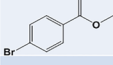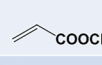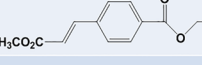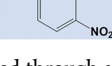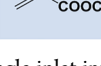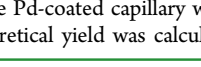
Figure 4. (a) Heck reaction equation. (b) Continuous microwave catalytic performance of Heck coupling using (1) the 3D Pd decorated network developed here, (2) the Pd network structure (prepared using the microstructure reported in ref 18 as the template), (3) the Pd nanowire array, and (4) the microchannel modified with Pd nanoparticles. (c) Recycling performance of the Pd network modified microchannel (each cycle had a continuous reaction time of 4 h). (d) Simulated and experimental catalytic performance. (e) Concentration variation of iodobenzene as a function of reaction time in the inlet of the channel (concentrations increase from blue to red).

contact areas. The inset in Figure 3b, suggests that the dimensions of the original porous networked substrate were retained; a result that is further confirmed upon examination of the tilted FE-SEM image (Figure 3c). As determined by high resolution FE-SEM analysis (Figure 3d and e), the decorated nanowires exhibited uniform surface roughness and nanoparticle distribution, which further confirmed the uniformity of Pd growth onto the pristine Zn(OH)F structures. FE-SEM-EDS elemental mapping analysis (Figure 3f), shows complete overlap of the two respective metal elements throughout the nanowire structure, demonstrating uniform Pd decoration. EDS

spectra provided additional details of the elemental composition (see Figure S3 in the Supporting Information).

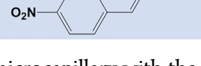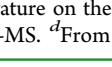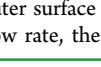TEM and HRTEM measurements facilitated investigation of the microstructure and in situ conversion mechanism. To clearly observe the nanocrystals on the original template surfaces, the growing network was imaged at a reaction time of 5 min. The TEM images (Figure 3g) reveal rough outer nanowire surfaces with uniformly distributed nanocrystals, which are estimated to be about 5 nm in diameter (HRTEM). Additionally, the lattice fringes are well correlated to representative (111) crystallographic planes. The d-spacing for adjacent lattice planes is 2.24 Å for the Pd nanocrystals,

Table 1. Microwave-Assisted Heck Coupling of Aryl Iodides and Aryl Bromides Using Flow and Batch Reactors under the Same Reaction Conditions

Heck Reaction							
				Flow Reactor		Batch Reactor	
Reagent A [a]	Reagent B [a]	Products	Temperature [b] (°C)	Time [e] (min)	Yield [c, d] (%)	Time [e] (min)	Yield [c, d] (%)
(4-CH₃O-phenyl iodide)	(CH₂=CH-COOCH₃)	(4-CH₃O-cinnamate)	180	3	89	60	78
(4-methyl phenyl iodide)	(CH₂=CH-COOCH₃)	(4-methyl cinnamate OCH₃)	185	3	91	60	76
(phenyl iodide)	(CH₂=CH-COO—C(CH₃)₂)	(tert-butyl cinnamate)	185	2	92	60	67
(phenyl iodide)	(CH₂=CH-CN)	(cinnamonitrile, CN)	185	2	94	60	81
(bromobenzene)	(styrene)	(stilbene)	135	2	81	60	52
(4-Br-phenyl, OEt vinyl)	(CH₂=CH-COOCH₃)	(H₃CO₂C—...—COO ethyl)	135	5	83	60	27
(4-Br-nitrophenyl)	(CH₂=CH-COOCH₃)	(O₂N—...—COOH)	135	3	85	60	34

[a]Reaction solutions flowed through a single inlet into a microcapillary with the 3D Pd decoratd network (12 cm) while being heated with microwave irradiation. [b]The temperature on the outer surface of the Pd-coated capillary was measured by using an IR sensor. [c]The yield was determined from capillary effluent by GC-MS. [d]From flow rate, the theoretical yield was calculated. [e]The reaction time was controlled by the pumping rate.

corresponding to the (111) planes of face-centered cubic (fcc) Pd (the *d*-spacing for the (111) planes of pure Pd is 2.24 Å).

To examine the electronic characteristics of the Pd decorated network, the binding energies for Pd 3d were characterized by X-ray photoelectron spectroscopy (XPS). The survey spectrum exhibited characteristic peaks corresponding to Zn and Pd photoemissions, which provide further evidence for the successful synthesis and growth of Pd on the original Zn(OH)F network. The binding energy for Pd 3d was 337.71 eV (Figure S4 in the Supporting Information), which confirms the in situ formation of a Pd⁰ network.[41] A PdPt alloy network was also prepared successfully via in situ chemical conversion using the 3D Zn(OH)F substrate. More details can be found in Figure S5 in the Supporting Information.

3.4. Typical Cross-Coupling Reaction Analysis. Pd modified microchannel performance was demonstrated using a representative Heck reaction (the reaction equation is shown in Figure 4a); microwave irradiation was used to improve reaction efficiency (control experiments performed without microwave irradiation can be found in Figure S6 in the Supporting Information). Microwave conditions are particularly attractive for flow chemistry reactions and higher reaction efficiency can be achieved.[42,43] The mechanism of microwave reaction-rate enhancement has been attributed to selective heating ("superheating") of the heterogeneous catalyst.[44,45]

Figure 4b presents a comparison of the conversion rate and percent yield for the reaction of iodobenzene and ethyl acrylate in a capillary system fabricated with Pd nanoparticles, Pd nanowire arrays, an alternative Pd decorated network (prepared using the microstructure reported in ref 13 as the template), and the 3D Pd decorated network developed here. The 3D Pd decorated network exhibited the best catalytic performance; the conversion reached 80% within 1 min vs merely 30−60% for the alternative systems. A conversion of almost 95% was achieved after only 3 min. The high catalytic performance can

be attributed to large fluid contact surface area. The large surface area with uniform and dense Pd decoration facilitated generation of more reaction sites.

The capillary based reaction process was simulated using commercial software (COMSOL Multiphysics 4.2). Using the shallow channel approximation,[46] microfluidic flow is governed by the following equations:

$$\rho(\nabla \cdot \mu) = 0 \qquad (3)$$

$$\rho(\mathbf{u} \cdot \nabla)\mathbf{u} = \nabla \cdot [-pI + \mu(\nabla \mathbf{u} + (\nabla \mathbf{u})^T)] - 12\frac{\mu \mathbf{u}}{d_z^2} \qquad (4)$$

The fluid flow was assumed to be steady state, and ρ and μ were obtained from the correlation of Yaws[47] based on DMF. The transport of chemical species can be written as

$$\frac{\partial c_i}{\partial t} + \mathbf{u} \cdot \nabla c_i + \nabla(-D_i \nabla c_i) = R_i \qquad (5)$$

where c_i is the concentration for each species and D_i is the diffusion coefficient. For simplicity, the reaction kinetics were assumed to be second order ($R = kc_{iodobenzene}c_{ethyl\ acrylate}$), where the kinetic constant k (0.001 m³ mol⁻¹ s⁻¹) was estimated from a fit to experimental data. Figure 4d presents a comparison of the conversion rate predicted by the model with the experimental data. The good agreement demonstrates that the relationship between the reaction rate and transport of chemical species by convection and diffusion is captured adequately with this simple model.

Figure 4e shows how the concentration of iodobenzene evolved in the channel inlet with time (the length shown in the figure is about 1.2 mm). Transport of iodobenzene to the network structure relied on diffusion, with the diffusion coefficient rising to about 10⁻⁸ m² s⁻¹ upon microwave heating. The corresponding diffusion time scale is r^2/D ca. 7 s. Therefore, at $t = 7$ s, iodobenzene had already infiltrated the

network. The simulation results (Figure 4e) also demonstrated that the flow-chemistry system was not mass-transport limited. Thus, the reaction rate is controlled by reaction kinetics. Compared with several alternative Pd-based microstructures (see Figure 4b), the Pd-based networks developed here exhibited optimized reaction kinetics. The analysis further suggested the advantages of the 3D structures in flow-chemistry catalysis.

During the flow process, while the reaction reached completion within 3 min, a 4 h continuous cycle was designed to characterize maximum reaction yield and robustness of the microchannel device. After continuous reaction for 1 cycle (about 4 h), the effluent was collected and analyzed by atomic emission spectroscopy to determine the durability of the Pd decorated structure. Only slightly elevated levels of Pd were detected (about 23 ppm) suggesting that Pd adheres well to the substrate and is not readily depleted. Figure 4c demonstrates that Pd modified microchannel performance is retained even after several reaction cycles. After continuous reaction for 5 cycles (about 20 h), reaction yields as high as 80% were achieved, providing supporting evidence of system structural and chemical stability. A slight decrease in the catalytic activity is noted during the cycles. The reason can be attributed to leaching of the metal, Pd nanoparticle aggregation and the formation of metal oxide. The results correspond well to the postrecycling microstructure characterization shown in Figure S7. Also, in comparison to what was observed with either batch or CSTR (continuous stirred tank reactors) processes,[48] minimal catalyst was detected in the product and no filtration was required.

The structural, morphological, and chemical integrity of the 3D Pd structure after recycling was further investigated using FE-SEM (Figure S7a). The 3D network survived the recycling process and good connectivity with the substrate was retained. In agreement with the recycling results, TEM and HRTEM analysis (Figure S7b and c) revealed only a small degree of Pd crystal growth and aggregation (Figure 4c). XPS spectra confirmed the near absence of metal oxide after recycling, which suggests that the 3D network has high antioxidant performance. More details can be found in the Supporting Information (Figure S7).

3.5. Flow-Chemistry System Versatility for Cross-Coupling Reactions. The versatility of the catalytic flow-chemistry system developed here was evaluated using a series of Heck and Suzuki−Miyaura reactions.

Heck Reaction. Table 1 compares the reaction times and associated yields for a series of Heck reactions. The 3D Pd decorated network exhibited high catalytic performance: under the flow conditions, consistently higher conversions with significantly shorter reactions times were achieved. Notably, aryl bromides also provided for high conversion with the continuous flow approach.[49] As seen in Table 1, for the same reaction parameters, under flow conditions, the aryl bromide coupling proceeded with yields consistently over 80% in just a few minutes, whereas batch reactor yields were in the range of only 25−50% for a reaction time of 1 h. Significant rate enhancement and improved yields can be obtained using the flow system. In addition, the 3D Pd decorated network is also effective in the case of Suzuki−Miyaura coupling reactions (Table S1 in the Supporting Information).

The results obtained for both Heck and Suzuki−Miyaura coupling reactions demonstrate the advantages derived from using the 3D microcapillary support structure designed and fabricated here. The highly networked structure, uniformly decorated with a Pd catalyst enabled a large surface area for the reaction and short diffusion distances. These elements provided for shorter reaction times and higher product yields. Further, high purity products were obtained. The approach is also expected to be scalable (more details can be found in Figure S8 in the Supporting Information).

4. CONCLUSION

In summary, a simple shear process that could be easily tuned for controlled growth of a diverse array of microstructures, for example, "fluid shear-induced microstructure formation", in confined microcapillaries was introduced for the first time. The resultant structures proved effective as substrates for the general synthesis of uniformly distributed 3D noble metal catalyst networks which exhibited high fluid contact area. Both mono- and multimetal networks were achieved; they were robust and withstood the physical "wear and tear" of flow conditions and the high temperatures associated with microwave irradiation. The catalytic performance of the Pd network was demonstrated for continuous-flow microwave-assisted Heck and Suzuki−Miyaura coupling reactions.

Fluid flow models supported the premise that shear forces combined with a highly networked microchannel based substrate microstructure allowed for growth of uniformly distributed catalyst on a substrate having high surface area. This synergistic combination of factors enabled the very efficient coupling of reactants. The ability to control micro-channel morphologies for desired performance attributes, together with the range of functionalities that could be introduced by in situ chemical conversion, could in the future enable the as yet still nascent areas of nanomanufacturing, microfluidic reaction processes, and functional microdevices.

■ ASSOCIATED CONTENT

Ⓢ Supporting Information

The Supporting Information is available free of charge on the ACS Publications website at DOI: 10.1021/acsami.5b06851.

> Details on the TEM and HETEM analysis of the Zn(OH)F network; temporal changes in the morphology of Pd decorated networks (TEM and HRTEM analysis); EDS spectrum of the in situ formed Pd network, XPS spectrum for the Pd 3d core level; FE-SEM, TEM, HRTEM, EDS, and XPS anlysis of PdPt networks; continuous catalytic performance of Heck coupling without microwave irradiation; morphology character-ization of the 3D Pd networks after recycling (FE-SEM, TEM, and XPS analysis); the scheme of scale-up experimental setup; schematic diagram of the continu-ous-flow microwave reaction system (PDF)

■ AUTHOR INFORMATION

Corresponding Authors
*E-mail: wanghz@dhu.edu.cn.
*E-mail: yaogang_li@dhu.edu.cn.
*E-mail: ereichmanis@chbe.gatech.edu.
Notes
The authors declare no competing financial interest.

■ ACKNOWLEDGMENTS

■ REFERENCES

(1) Hartman, R. L.; McMullen, J. P.; Jensen, K. F. Deciding Whether to Go with the Flow: Evaluating the Merits of Flow Reactors for Synthesis. *Angew. Chem., Int. Ed.* **2011**, *50*, 7502−7519.

(2) Shore, G.; Morin, S.; Organ, M. G. Catalysis in Capillaries by Pd Thin Films Using Microwave-Assisted Continuous-Flow Organic Synthesis (MACOS). *Angew. Chem.* **2006**, *118*, 2827−2832.

(3) Chen, X.; Smith, N. M.; Iyer, K. S.; Raston, C. L. Controlling Nanomaterial Synthesis, Chemical Reactions and Self Assembly in Dynamic Thin Films. *Chem. Soc. Rev.* **2014**, *43*, 1387−1399.

(4) Wirth, T. *Microreactors in Organic Chemistry and Catalysis*, 1st ed.; John Wiley & Sons: Hoboken, NJ, 2008.

(5) Wang, H.; Nakamura, H.; Miyazaki, M.; Maeda, H. Continuous Particle Self-Arrangement in a Long Microcapillary. *Adv. Mater.* **2002**, *14*, 1662−1666.

(6) He, Z. Y.; Li, Y. G.; Zhang, Q. H.; Wang, H. Z. Capillary Microchannel-based Microreactors with Highly Durable ZnO/TiO₂ Nanorod Arrays for Rapid, High Efficiency and Continuous-flow Photocatalysis. *Appl. Catal., B* **2010**, *93*, 376−382.

(7) Wang, G.; He, Z.; Shi, G.; Wang, H.; Zhang, Q.; Li, Y. Controllable Construction of Titanium Dioxide-Zirconium Dioxide@ Zinc Hydroxyfluoride Networks in Micro-capillaries for Bio-analysis. *J. Colloid Interface Sci.* **2015**, *446*, 290−297.

(8) Chernyak, N.; Buchwald, S. L. Continuous-Flow Synthesis of Monoarylated Acetaldehydes Using Aryldiazonium Salts. *J. Am. Chem. Soc.* **2012**, *134*, 12466−12469.

(9) Rodrigues, T.; Schneider, P.; Schneider, G. Accessing New Chemical Entities through Microfluidic Systems. *Angew. Chem., Int. Ed.* **2014**, *53*, 5750−5758.

(10) Noel, T.; Naber, J. R.; Hartman, R. L.; McMullen, J. P.; Jensen, K. F.; Buchwald, S. L. Palladium-catalyzed Amination Reactions in Flow: Overcoming the Challenges of Clogging *via* Acoustic Irradiation. *Chem. Sci.* **2011**, *2*, 287−290.

(11) Nikbin, N.; Ladlow, M.; Ley, S. V. Continuous Flow Ligand-Free Heck Reactions Using Monolithic Pd [0] Nanoparticles. *Org. Process Res. Dev.* **2007**, *11*, 458−462.

(12) Newman, S. G.; Jensen, K. F. The Role of Flow in Green Chemistry and Engineering. *Green Chem.* **2013**, *15*, 1456−1472.

(13) Nagaki, A.; Moriwaki, Y.; Yoshida, J. I. Flow Synthesis of Arylboronic Esters Bearing Electrophilic Functional Groups and Space Integration with Suzuki−Miyaura Coupling without Intentionally Added Base. *Chem. Commun.* **2012**, *48*, 11211−11213.

(14) Wegner, J.; Ceylan, S.; Kirschning, A. Ten Key Issues in Modern Flow Chemistry. *Chem. Commun.* **2011**, *47*, 4583−4592.

(15) Wang, L.; Ma, S.; Wang, X.; Bi, H.; Han, X. Mixing Enhancement of a Passive Microfluidic Mixer Containing Triangle Baffles. *Asia-Pac. J. Chem. Eng.* **2014**, *9*, 877−885.

(16) McQuade, D. T.; Seeberger, P. H. Applying Flow Chemistry: Methods, Materials, and Multistep Synthesis. *J. Org. Chem.* **2013**, *78*, 6384−6389.

(17) Huang, Q. L.; Wang, M.; Zhong, H. X.; Chen, X. T.; Xue, Z. L.; You, X. Z. Netlike Nanostructures of Zn(OH)F and ZnO: Synthesis, Characterization, and Properties. *Cryst. Growth Des.* **2008**, *8*, 1412−1417.

(18) Wang, G.; Shi, G.; Wang, H.; Zhang, Q.; Li, Y. In Situ Functionalization of Stable 3D Nest-Like Networks in Confined Channels for Microfluidic Enrichment and Detection. *Adv. Funct. Mater.* **2014**, *24*, 1017−1026.

(19) Hansen, T. W.; DeLaRiva, A. T.; Challa, S. R.; Datye, A. K. Sintering of Catalytic Nanoparticles: Particle Migration or Ostwald Ripening? *Acc. Chem. Res.* **2013**, *46*, 1720−1730.

(20) Tan, S.; Sun, X. J.; Williams, C. T. In Situ ATR-IR Study of Prochiral 2-methyl-2-Pentenoic Acid Adsorption on Al₂O₃ and Pd/ Al₂O₃. *Phys. Chem. Chem. Phys.* **2011**, *13*, 19573−19579.

(21) Du, W.; Yang, G.; Wong, E.; Deskins, N. A.; Frenkel, A. I.; Su, D.; Teng, X. Platinum-Tin Oxide Core−Shell Catalysts for Efficient Electro-Oxidation of Ethanol. *J. Am. Chem. Soc.* **2014**, *136*, 10862−10865.

(22) Wan, Y.; Wang, H.; Zhao, Q.; Klingstedt, M.; Terasaki, O.; Zhao, D. Ordered Mesoporous Pd/Silica−Carbon as a Highly Active Heterogeneous Catalyst for Coupling Reaction of Chlorobenzene in Aqueous Media. *J. Am. Chem. Soc.* **2009**, *131*, 4541−4550.

(23) Modak, A.; Mondal, J.; Sasidharan, M.; Bhaumik, A. Triazine Functionalized Ordered Mesoporous Polymer: a Novel Solid Support for Pd-mediated C−C Cross-coupling Reactions in Water. *Green Chem.* **2011**, *13*, 1317−1331.

(24) Lim, M. A.; Kim, D. H.; Park, C.-O.; Lee, Y. W.; Han, S. W.; Li, Z.; Williams, R. S.; Park, I. A New Route toward Ultrasensitive, Flexible Chemical Sensors: Metal Nanotubes by Wet-Chemical Synthesis along Sacrificial Nanowire Templates. *ACS Nano* **2012**, *6*, 598−608.

(25) Chng, L. L.; Erathodiyil, N.; Ying, J. Y. Nanostructured Catalysts for Organic Transformations. *Acc. Chem. Res.* **2013**, *46*, 1825−1837.

(26) Teng, X.; Maksimuk, S.; Frommer, S.; Yang, H. Three-dimensional PtRu Nanostructures. *Chem. Mater.* **2007**, *19*, 36−41.

(27) Uozumi, Y.; Yamada, Y. M.; Beppu, T.; Fukuyama, N.; Ueno, M.; Kitamori, T. Instantaneous Carbon−Carbon Bond Formation Using a Microchannel Reactor with a Catalytic Membrane. *J. Am. Chem. Soc.* **2006**, *128*, 15994−15995.

(28) Yamada, Y.; Watanabe, T.; Beppu, T.; Fukuyama, N.; Torii, K.; Uozumi, Y. Palladium Membrane-Installed Microchannel Devices for Instantaneous Suzuki−Miyaura Cross-Coupling. *Chem. - Eur. J.* **2010**, *16*, 11311−11319.

(29) Seong, G. H.; Crooks, R. M. Efficient Mixing and Reactions within Microfluidic Channels Using Microbead-Supported Catalysts. *J. Am. Chem. Soc.* **2002**, *124*, 13360−13361.

(30) Yang, Z.; Zhou, X.; Jin, Z.; Liu, Z.; Nie, H.; Chen, X. A.; Huang, S. A Facile and General Approach for the Direct Fabrication of 3D, Vertically Aligned Carbon Nanotube Array/Transition Metal Oxide Composites as Non-Pt Catalysts for Oxygen Reduction Reactions. *Adv. Mater.* **2014**, *26*, 3156−3161.

(31) Goh, Y. A.; Chen, X.; Yasin, F. M.; Eggers, P. K.; Boulos, R. A.; Wang, X.; Chua, H. T.; Raston, C. L. Shear Flow Assisted Decoration of Carbon Nano-onions with Platinum Nanoparticles. *Chem. Commun.* **2013**, *49*, 5171−5173.

(32) Sun, J.; Xianyu, Y.; Jiang, X. Point-of-care Biochemical Assays Using Gold Nanoparticle-implemented Microfluidics. *Chem. Soc. Rev.* **2014**, *43*, 6239−6253.

(33) Zarzar, L. D.; Swartzentruber, B. S.; Harper, J. C.; Dunphy, D. R.; Brinker, C. J.; Aizenberg, J.; Kaehr, B. Multiphoton Lithography of Nanocrystalline Platinum and Palladium for Site-Specific Catalysis in 3D Microenvironments. *J. Am. Chem. Soc.* **2012**, *134*, 4007−4010.

(34) Luo, C.; Kyaw, K. K.; Perez, L.A.; Patel, S.; Wang, M.; Grimm, B.; Bazan, G. C.; Kramer, E. J.; Heeger, A. J. General Strategy for Self-Assembly of Highly Oriented Nanocrystalline Semiconducting Polymers with High Mobility. *Nano Lett.* **2014**, *14*, 2764−2771.

(35) Chang, C.-H.; Wu, C.-E.; Chen, S.-Y.; Cui, C.; Cheng, Y.-J.; Hsu, C.-S.; Wang, Y.-L.; Li, Y. Enhanced Performance and Stability of a Polymer Solar Cell by Incorporation of Vertically Aligned, Cross-Linked Fullerene Nanorods. *Angew. Chem., Int. Ed.* **2011**, *50*, 9386−9390.

(36) Liu, J. W.; Zheng, J.; Wang, J. L.; Xu, J.; Li, H. H.; Yu, S. H. Ultrathin W₁₈O₄₉ Nanowire Assemblies for Electrochromic Devices. *Nano Lett.* **2013**, *13*, 3589−3593.

(37) Diao, Y.; Tee, B. C. K.; Giri, G.; Xu, J.; Kim, D. H.; Becerril, H. A.; Stoltenberg, R. M.; Lee, T. H.; Xue, G.; Mannsfeld, S. C. B.; Bao, Z. Solution Coating of Large-area Organic Semiconductor Thin films with Aligned Single-crystalline Domains. *Nat. Mater.* **2013**, *12*, 665−671.

(38) Varagnolo, S.; Ferraro, D.; Fantinel, P.; Pierno, M.; Mistura, G.; Amati, G.; Biferale, L.; Sbragaglia, M. Stick-Slip Sliding of Water Drops on Chemically Heterogeneous Surfaces. *Phys. Rev. Lett.* **2013**, *111*, 066101.

(39) Amini, H.; Sollier, E.; Masaeli, M.; Xie, Y.; Ganapathysubramanian, B.; Stone, H. A.; Di Carlo, D. Engineering Fluid Flow Using Sequenced Microstructures. *Nat. Commun.* **2013**, *4*, 1826.

(40) Watanabe, K.; Udagawa, Y.; Udagawa, H. Drag Reduction of Newtonian Fluid in a Circular Pipe with a Highly Water-repellent Wall. *J. Fluid Mech.* **1999**, *381*, 225−238.

(41) Liqiang, J.; Dejun, W.; Baiqi, W.; Shudan, L.; Baifu, X.; Honggang, F.; Jiazhong, S. Effects of Noble Metal Modification on Surface Oxygen Composition, Charge Separation and Photocatalytic Activity of ZnO Nanoparticles. *J. Mol. Catal. A: Chem.* **2006**, *244*, 193−200.

(42) Kappe, C. O. Controlled Microwave Heating in Modern Organic Synthesis. *Angew. Chem., Int. Ed.* **2004**, *43*, 6250−6284.

(43) Kappe, C. O.; Pieber, B.; Dallinger, D. Microwave Effects in Organic Synthesis: Myth or Reality? *Angew. Chem., Int. Ed.* **2013**, *52*, 1088−1094.

(44) Comer, E.; Organ, M. G. A Microreactor for Microwave-Assisted Capillary (Continuous Flow) Organic Synthesis. *J. Am. Chem. Soc.* **2005**, *127*, 8160−8167.

(45) Leadbeater, N. E. *Microwave Heating As a Tool for Sustainable Chemistry*, 1st ed.; CRC Press: Boca Raton, FL, 2011.

(46) Yaws, C. L. *Thermophysical Properties of Chemicals and Hydrocarbons*, 1st ed.; William Andrew Publishing: Norwich, NY, 2008.

(47) Yaws, C. L. *Yaws' Handbook of Thermodynamic and Physical Properties of Chemical Compounds*, 1st ed.; Knovel Co.: Norwich, NY, 2003.

(48) Chilin, D.; Liu, J.; Chen, X.; Christofides, P. D. Fault Detection and Isolation and Fault Tolerant Control of a Catalytic Alkylation of Benzene Process. *Chem. Eng. Sci.* **2012**, *78*, 155−166.

(49) Anbarasan, P.; Schareina, T.; Beller, M. Recent Developments and Perspectives in Palladium-catalyzed Cyanation of Aryl Halides: Synthesis of Benzonitriles. *Chem. Soc. Rev.* **2011**, *40*, 5049−5067.